LETTERS TO THE EDITOR

This Letters section is for publishing (a) brief acoustical research or applied acoustical reports, (b) comments on articles or letters previously published in this Journal, and (c) a reply by the article author to criticism by the Letter author in (b). Extensive reports should be submitted as articles, not in a letter series. Letters are peer-reviewed on the same basis as articles, but usually require less review time before acceptance. Letters cannot exceed four printed pages (approximately 3000–4000 words) including figures, tables, references, and a required abstract of about 100 words.

Scattering by an arrangement of eccentric cylinders embedded on a coated cylinder with applications to tomographic density imaging (L)

Roberto J. Lavarello[a] and Michael L. Oelze
Department of Electrical and Computer Engineering, Bioacoustics Research Laboratory, University of Illinois at Urbana-Champaign, 405 North Matthews, Urbana, Illinois 61801

(Received 10 August 2009; revised 22 November 2009; accepted 23 November 2009)

The solution to the scattering of an incident pressure wave by an arrangement of eccentric cylinders embedded inside a pair of concentric cylinders is derived here using a combination of T-matrix and mode-matching approaches. This method allows the generation of synthetic data from relatively complex structures to be used for the validation of acoustic tomography methods. An application of the solution derived here is illustrated by reconstructing sound speed and density profiles from a complex phantom using inverse scattering. © *2010 Acoustical Society of America.*
[DOI: 10.1121/1.3277154]

PACS number(s): 43.20.Fn, 43.35.Wa [TDM] Pages: 645–648

I. INTRODUCTION

The scattering of a cylindrical wave by an arrangement of eccentric cylinders is derived here in order to validate inverse scattering routines with scatterers more complex than a single homogeneous cylinder. Works dealing with the scattering by two concentric fluid cylinders,[1] two[2] and multiple[3] rigid parallel cylinders, two[4] and multiple[5] fluid parallel cylinders, two eccentric fluid cylinders,[6,7] and multiple eccentric cylinders embedded in a circular cylinder[8] can be found in the literature. The work presented here extends the scope of the work in Ref. 8 by studying the scattering by N circular cylinders embedded inside a coated cylinder, as shown in Fig. 1.

The approach presented here is a combination of the T-matrix formulation and mode-matching techniques, and considers changes in compressibility, density, and attenuation (unlike the work in Ref. 8 that only considers changes in refractive index).

II. CALCULATION OF THE SCATTERING COEFFICIENTS

In the following derivation, the background has a wave number k_0 and acoustic impedance Z_0. For the other cylinders, the complex wave numbers k_n and impedances Z_n are defined as $k_n=(\omega/c_n)+i\alpha_n$ and $Z_n=\rho_n c_n/(1+i\alpha_n c_n/\omega)$, where c_n, ρ_n, and α_n are the speed of sound, density, and attenuation coefficient in the n-th subregion. The radius of the n-th cylinder is denoted by a_n. The wave number, impedance, and outer radius of the coating are denoted by k_c, Z_c, and a_c, respectively. The acoustic field inside cylinder 1 can be written as

$$p_1(\vec{r}_o)=\sum_{m=-\infty}^{\infty} A_m J_m(k_1 r_o)e^{im\theta_o} + \sum_{n=2}^{N+1}\sum_{p=-\infty}^{\infty} B_{p,n}H_p(k_1 r_{on})e^{ip\theta_{on}}, \tag{1}$$

where $J_m(\cdot)$ is the m-th order Bessel function, $H_m(\cdot)$ is the m-th order Hankel function of the first kind, $\vec{r}_o=(r_o,\theta_o)$ are the polar coordinates of the observation point, $\vec{r}_n=(r_n,\theta_n)$ are the polar coordinates of the center of the n-th cylinder, and $\vec{r}_{on}=\vec{r}_o-\vec{r}_n$. The second sum in Eq. (1) represents the fields produced by the embedded cylinders. The T-matrix approach[9] can be used to relate the amplitudes of the A_m and $B_{p,n}$ terms. First, a matrix $\bar{T}_s$ is used to express the Bessel waves relative to the center of each one of the N embedded cylinders. The matrix $\bar{T}_s$ is composed of M blocks $\bar{T}_s^h$ of size $N\times M_p$, where M and M_p are the number of terms used to expand the first and second infinite sums in Eq. (1). This can be expressed in matrix form as

$$\bar{e}_t=\bar{T}_s\cdot\bar{a}, \tag{2}$$

$$\bar{T}_s=[\cdots\ (\bar{T}_s^{m=-1})^T\ (\bar{T}_s^{m=0})^T\ (\bar{T}_s^{m=1})^T\ \cdots]^T, \tag{3}$$

[a]Author to whom correspondence should be addressed. Electronic mail: lavarell@illinois.edu

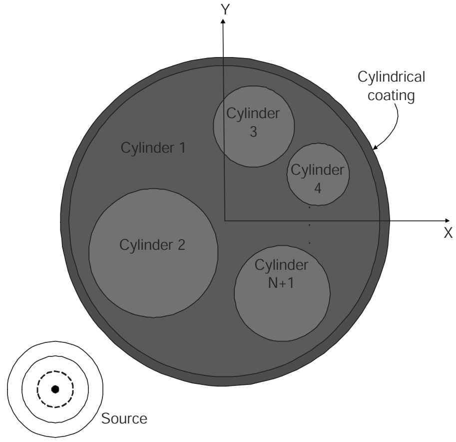

FIG. 1. Scatterer formed by an arrangement of circular cylinders embedded inside a coated circular cylinder.

$$[\bar{T}_s^n]_{np} = J_{p-m}(k_1 r_n) e^{-i(p-m)(\theta_n+\pi)}, \tag{4}$$

where $\bar{a}$ is an M_p length vector with the amplitudes of the Bessel wave harmonics and $\bar{e}_t$ is an $(M\times N)$ vector with the translated amplitudes of the Bessel waves. In the notation above, $\bar{X}^T$ represents the transpose of a matrix $\bar{X}$. The harmonics $\bar{e}_t$ can be related to the Hankel harmonics in Eq. (1) as

$$\bar{b}_t = [\bar{I} - \mathcal{D}(\bar{R})\cdot\bar{A}]^{-1}\cdot\mathcal{D}(\bar{R})\cdot\bar{e}_t. \tag{5}$$

where $\bar{b}_t$ is an $(M\times N)$ vector with the $B_{p,n}$ coefficients and $\mathcal{D}(\cdot)$ is an operator that transforms a vector into a diagonal matrix. The $(M\times N)$ vector $\bar{R}$ contains the single-cylinder scattering coefficients given by

$$\bar{R} = [(\bar{R}^{n=2})^T\ (\bar{R}^{n=3})^T\ \cdots\ (\bar{R}^{n=N+1})^T]^T, \tag{6}$$

$$[\bar{R}^n]_p = \frac{\frac{1}{Z_{rn}} J_p(k_1 a_n) J'_p(k_n a_n) - J_p(k_n a_n) J'_p(k_1 a_n)}{J_p(k_n a_n) H'_p(k_1 a_n) - \frac{1}{Z_{rn}} J'_p(k_n a_n) H_p(k_1 a_n)}, \tag{7}$$

where the "$'$" symbol denotes derivative with respect to the total argument and $Z_{rn}=Z_n/Z_1$. The elements of the $(M\times N)\times(M\times N)$ T-matrix $\bar{A}$ are given by

$$\bar{A} = \begin{bmatrix} \bar{A}_{11} & \bar{A}_{12} & \cdots & \bar{A}_{1M} \\ \bar{A}_{21} & \bar{A}_{22} & \cdots & \bar{A}_{2M} \\ & \vdots & & \\ \bar{A}_{M1} & \bar{A}_{M2} & \cdots & \bar{A}_{MM} \end{bmatrix}, \tag{8}$$

$$[\bar{A}_{mn}]_{pq} = \begin{cases} 0 & \text{if } p=q \\ H_{m-n}(k_0 r_{pq}) e^{-i(m-n)\theta_{pq}}, & \text{else,} \end{cases} \tag{9}$$

where (r_{pq},θ_{pq}) is the polar representation of the vector $(\vec{r}_p - \vec{r}_q)$ containing the location of the center of cylinder p relative to the center of cylinder q, with $p,q\in[2,N+1]$. Enforcing mode-matching at the cylindrical coating becomes simpler if Eq. (1) is expressed in terms of Bessel and Hankel fields centered at the origin. In particular, if the observation point $\vec{r}_o$ satisfies $|\vec{r}_o|>|\vec{r}_n|$, $\forall n\in[2,N+1]$, the addition theorem of Hankel functions[10] allows the pressure field to be expressed as

$$p_1(\vec{r}_o) = \sum_{m=-\infty}^{\infty} (A_m J_m(k_1 r_o) + B_m H_m^{(1)}(k_1 r_o)) e^{im\theta_o}, \tag{10}$$

where the relationship between the B_m and $B_{p,n}$ coefficients is given by

$$\bar{b} = \bar{T}\cdot\bar{b}_t, \tag{11}$$

$$\bar{T} = [\cdots\ \bar{T}^{h=-1}\ \bar{T}^{h=0}\ \bar{T}^{h=1}\ \cdots], \tag{12}$$

$$[\bar{T}^{h=m}]_{pn} = J_{p-m}(k_1 r_n) e^{-i(p-m)\theta_n}, \tag{13}$$

where $\bar{T}$ is an $(M\times P)\times(M\times M)$ transition matrix, and $\bar{b}$ is an M_p length vector containing the coefficients B_m. Overall, the relationship between the A_m and B_m coefficients can be expressed as

$$\bar{b} = \bar{P}\cdot\bar{a},$$

$$\bar{P} = \bar{T}\cdot[\bar{I} - \mathcal{D}(\bar{R})\cdot\bar{A}]^{-1}\cdot\mathcal{D}(\bar{R})\cdot\bar{T}_s. \tag{14}$$

The expression in Eq. (14) is valid, in particular, for points close to the edge of cylinder 1. In the cylindrical coating, the field can be expressed as

$$p(\vec{r}_o) = \sum_{m=-\infty}^{\infty} (C_m J_m(k_c r_o) + D_m H_m(k_c r_o)) e^{im\theta_o}, \tag{15}$$

where the first sum is the incident field and the second one is the scattered field. The magnitudes of the A_m, B_m, C_m, and D_m coefficients can be related using the continuity of both pressure and normal particle velocity at $r_o=a_1$. Therefore, one can express

$$\mathcal{D}(\bar{R}_{jj})\cdot\bar{a} + \mathcal{D}(\bar{R}_{hj})\cdot\bar{b} = \bar{c}, \tag{16}$$

$$\mathcal{D}(\bar{R}_{jh})\cdot\bar{a} + \mathcal{D}(\bar{R}_{hh})\cdot\bar{b} = \bar{d}, \tag{17}$$

where $\bar{c}$ and $\bar{d}$ are M_p length vectors with the coefficients C_m and D_m, respectively, and $\bar{R}_{jj}$, $\bar{R}_{hj}$, $\bar{R}_{jh}$, and $\bar{R}_{hh}$ are M_p length vectors containing the transmission coefficients given by

$$[\bar{R}_{jj}]_m = \frac{J_m(k_1 a_1) H'_m(k_c a_1) - \frac{1}{Z_{rc}} J'_m(k_1 a_1) H_m(k_c a_1)}{J_m(k_c a_1) H'_m(k_c a_1) - J'_m(k_c a_1) H_m(k_c a_1)}, \tag{18}$$

$$[\bar{R}_{hj}]_m = \frac{H_m(k_1 a_1) H'_m(k_c a_1) - \frac{1}{Z_{rc}} H'_m(k_1 a_1) H_m(k_c a_1)}{J_m(k_c a_1) H'_m(k_c a_1) - J'_m(k_c a_1) H_m(k_c a_1)}, \tag{19}$$

$$[\bar{R}_{hj}]_m = -\frac{J_m(k_1 a_1) J'_m(k_c a_1) - \frac{1}{Z_{rc}} J'_m(k_1 a_1) J_m(k_c a_1)}{J_m(k_c a_1) H'_m(k_c a_1) - J'_m(k_c a_1) H_m(k_c a_1)}, \tag{20}$$

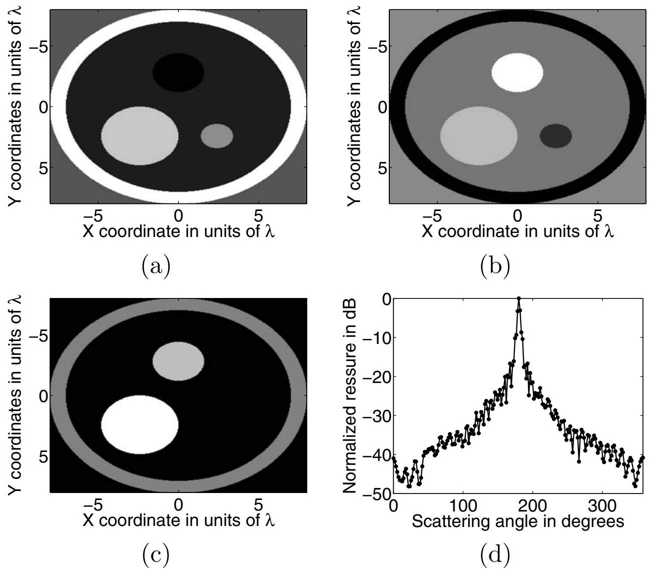

FIG. 2. Numerical validation of the scattering solution. (a) Δc of the phantom. (b) $\Delta\rho$ of the phantom. (c) Ratio α/k_0 of the phantom. (c) Scattered field produced by the phantom calculated using the solution presented in Sec. II (solid) and the numerical solver from Ref. 11 (dots).

$$[\bar{R}_{hh}]_m = \frac{\frac{1}{Z_{rc}} H'_m(k_1 a_1) J_m(k_c a_1) - H_m(k_1 a_1) J'_m(k_c a_1)}{J_m(k_c a_1) H'_m(k_c a_1) - J'_m(k_c a_1) H_m(k_c a_1)}, \quad (21)$$

where $Z_{rc}=Z_1/Z_c$. Similarly, the field in the background can be written as

$$p(\vec{r}_o) = \sum_{m=-\infty}^{\infty} (E_m J_m(k_0 r_o) + F_m H_m(k_0 r_o)) e^{im\theta_o}, \quad (22)$$

where the first term represents the incident field and the second term represents the scattered field. The coefficients E_m are known and depend on the type of illumination used. For example, when using a line source located at $\vec{R}_s(R_s,\theta_s)$ the coefficients E_m are given by $E_m=H_m^{(1)}(k_0 R_s)e^{-im\theta_s}$. The coefficients F_m are the unknowns that need to be solved in order to calculate the scattered field. The relationships between the coefficients C_m, D_m, E_m, and F_m are given by

$$\mathcal{D}(\bar{R}_{jj2}) \cdot \bar{c} + \mathcal{D}(\bar{R}_{hj2}) \cdot \bar{d} = \bar{e}, \quad (23)$$

$$\mathcal{D}(\bar{R}_{jh2}) \cdot \bar{c} + \mathcal{D}(\bar{R}_{hh2}) \cdot \bar{d} = \bar{f}, \quad (24)$$

where $\bar{e}$ and $\bar{f}$ are M_p length vectors containing the E_m and F_m coefficients, respectively, and the transmission coefficients $\bar{R}_{jj2}$, $\bar{R}_{hj2}$, $\bar{R}_{jh2}$, and $\bar{R}_{hh2}$ can be found using Eqs. (18)–(21) replacing a_1 by a_c, k_c by k_0, k_1 by k_c, and Z_{rc} by Z_c/Z_0. Therefore, the A_m coefficients can be found by using

$$\bar{a} = [\mathcal{D}(\bar{R}_{jj2}) \cdot \bar{M}_1 + \mathcal{D}(\bar{R}_{hj2}) \cdot \bar{M}_2]^{-1} \cdot \bar{e}, \quad (25)$$

$$\bar{M}_1 = \mathcal{D}(\bar{R}_{jj}) + \mathcal{D}(\bar{R}_{hj}) \cdot \bar{P}, \quad (26)$$

$$\bar{M}_2 = \mathcal{D}(\bar{R}_{jh}) + \mathcal{D}(\bar{R}_{hh}) \cdot \bar{P}. \quad (27)$$

Finally, the scattering coefficients F_m can be obtained by using

$$\bar{f} = [\mathcal{D}(\bar{R}_{jh2}) \cdot \bar{M}_1 + \mathcal{D}(\bar{R}_{hh2}) \cdot \bar{M}_2] \cdot \bar{a}. \quad (28)$$

These coefficients F_m are the ones needed to calculate the scattered field using the second term in Eq. (22).

TABLE I. Properties of the scatterer used for numerical validation of the scattering solution from Sec. II.

Cylinder	Center	Radius	Δc (%)	$\Delta\rho$ (%)	α/k
1	[0,0]	$8\lambda_0$ (outer) $7\lambda_0$ (inner)	6	−6	0.1
2	[0,0]	$7\lambda_0$	−2	−1	0
3	$[0, 2.8\lambda_0]$	$1.6\lambda_0$	−3	5	0.15
4	$[-2.4\lambda_0, -2.4\lambda_0]$	$2.4\lambda_0$	4	2	0.2
5	$[2.4\lambda_0, -2.4\lambda_0]$	λ_0	2	−4	0

III. NUMERICAL VALIDATION

An example of the scattering solution derived in this work is shown in Fig. 2. The dimensions, speed of sound, and density contrasts Δc and $\Delta\rho$, and α/k ratios of all cylinders are given in Table I. The incident field was produced by a line source located at $x=300\lambda$. The values of M and M_p for the scattering solution were set to 51 and 121, respectively. The scattered field was also calculated using the numerical solver presented in Ref. 11 with a grid size of $\lambda/20$. The root mean square error between both calculated scattered fields was only 0.4%, which suggests a proper convergence of the solution derived in this manuscript even in the presence of attenuation. The results are shown in Fig. 2.

Although in principle there should be no restrictions on the sizes and acoustic properties of the embedded cylinders as long as they remain nonoverlapping, special care must be taken when reconstructing scatterers consisting of regions

TABLE II. Mean speed of sound and density values corresponding to the reconstruction of a complex scatterer using the multiple frequency T-matrix approach with different $f_{\min}$ values.

Cylinder No.	Center position	Radius	$(\Delta c, \Delta\rho)$ ideal	$(\Delta c, \Delta\rho)$ $f_{\min}=f_0$	$(\Delta c, \Delta\rho)$ $f_{\min}=f_0/16$	$(\Delta c, \Delta\rho)$ $f_{\min}=f_0/64$
1	[0,0]	$8\lambda_0$ (outer) $7\lambda_0$ (inner)	(1.8%, −1.5%)	(1.68%, −2.5%)	(1.6%, −1.31%)	(1.6%, −1.51%)
2	[0,0]	$7\lambda_0$	(−1.8%, 1.5%)	(−1.78%, 2.88%)	(−1.76%, 2.09%)	(−1.76%, 1.67%)
3	$[1.8\lambda_0, 1.8\lambda_0]$	$2\lambda_0$	(2.5%, −2%)	(2.36%, −3.56%)	(2.32%, −1.61%)	(2.32%, −2.13%)
4	$[-2.4\lambda_0, -2.4\lambda_0]$	$1.6\lambda_0$	(−2.5%, 2%)	(−2.49%, 4.11%)	(−2.48%, 2.99%)	(−2.49%, 2.34%)

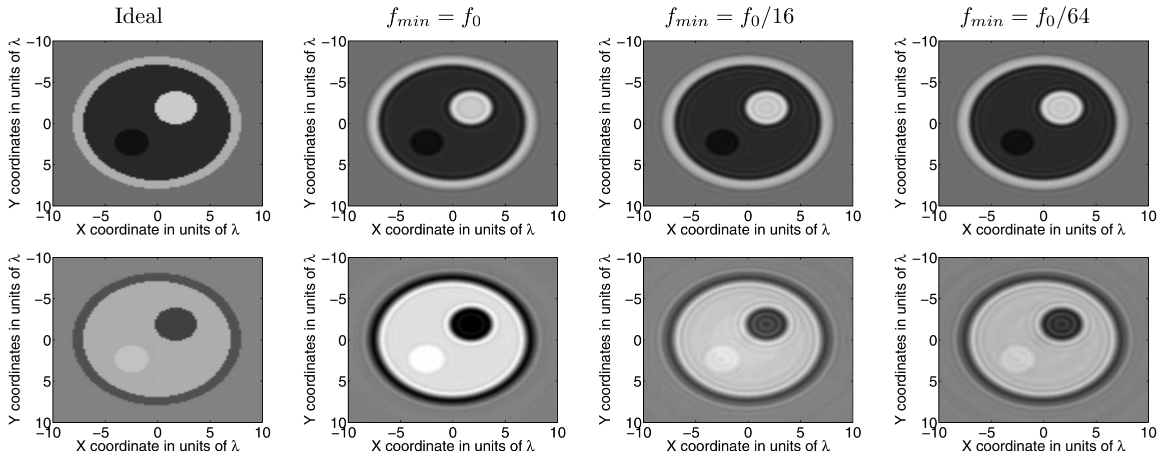

FIG. 3. Speed of sound (top row) and density (bottom row) images obtained using the multiple frequency T-matrix approach. First column: ideal profiles. Second columns: reconstructions using $f_{\min}$ values of f_0, $f_0/16$, and $f_0/64$, respectively.

that exhibit markedly different sizes or acoustic contrasts. In these cases, the finite precision of currently available floating-point arithmetic systems may prevent the proper computation and inversion of all the matrices involved in the solution presented in Sec. II.

IV. APPLICATION TO INVERSE SCATTERING PROBLEMS

The scattering solution presented in Sec. II was used to generate synthetic scattered data from a complex object in order to perform density imaging using the multiple frequency T-matrix approach.[11] The performance of this method when imaging homogeneous cylindrical objects has been reported previously.[12] Data were generated at frequencies $f_0, f_0/2, f_0/4, \ldots, f_{\min}$ and processed sequentially starting from the minimum frequency $f_{\min}$. Details of the implementation of the algorithm are given in Ref. 12. The properties and mean reconstructed values for all cylinders using $f_{\min}$ values of f_0, $f_0/16$, and $f_0/64$ are given in Table II. The reconstructions are shown in Fig. 3.

The speed of sound reconstructions exhibited high numerical accuracy independently of the value of $f_{\min}$. As for the density reconstructions, the maximum reduction in the bias between the ideal and reconstructed density values for a homogeneous circular cylinder of radius a should occur when $k_{\min}a \approx 1$ according to the results in Ref. 12. Therefore, the cylindrical inclusions of radius $1.6\lambda_0$ and $2\lambda_0$ should already exhibit the minimum achievable bias when using $f_{\min} = f_0/16$. However, the bias was reduced even further when using $f_{\min} = f_0/64$. Therefore, these results suggest that the absolute density values of a complex imaging target may not be obtained unless convergence is guaranteed for the overall structure when using the T-matrix approach.

V. CONCLUSIONS

The solution for the scattering produced by multiple parallel cylinders embedded inside a coated cylinder taking into account changes in compressibility, density, and acoustic attenuation has been presented. The applicability of the scattering solution presented here was demonstrated by analyzing the convergence of a method for variable density inverse scattering when imaging objects with multiple levels of spatial variations.

[1] J. Sinai and R. C. Waag, "Ultrasonic scattering by two concentric cylinders," J. Acoust. Soc. Am. **83**, 1728–1735 (1988).
[2] J. W. Young and J. C. Bertrand, "Multiple scattering by two cylinders," J. Acoust. Soc. Am. **58**, 1190–1195 (1975).
[3] S. E. Sherer, "Scattering of sound from axisymetric sources by multiple circular cylinders," J. Acoust. Soc. Am. **115**, 488–496 (2004).
[4] J. A. Roumeliotis, A.-G. P. Ziotopoulos, and G. C. Kokkorakis, "Acoustic scattering by a circular cylinder parallel with another of small radius," J. Acoust. Soc. Am. **109**, 870–877 (2001).
[5] V. Twersky, "Multiple scattering of radiation by an arbitrary configuration of parallel cylinders," J. Acoust. Soc. Am. **24**, 42–46 (1952).
[6] N. K. Uzunoglu and J. G. Fikioris, "Scattering from an infinite dielectric cylinder embedded into another," J. Phys. A **12**, 825–834 (1979).
[7] R. P. Parrikar, A. A. Kishk, and A. Z. Elsherbeni, "Scattering from an impedance cylinder embedded in a nonconcentric dielectric cylinder," IEE Proc. Microwaves, Antennas Propag. **138**, 169–175 (1991).
[8] L. G. Stratigaki, M. P. Ioannidou, and D. P. Chrissoulidis, "Scattering from a dielectric cylinder with multiple eccentric cylindrical dielectric inclusions," IEE Proc. Microwaves, Antennas Propag. **143**, 505–511 (1996).
[9] P. C. Waterman, "New formulation of acoustic scattering," J. Acoust. Soc. Am. **45**, 1417–1429 (1969).
[10] W. C. Chew, *Waves and Fields in Inhomogeneous Media* (IEEE, Piscataway, NJ, 1995).
[11] J. Lin and W. Chew, "Ultrasonic imaging by local shape function method with CGFFT," IEEE Trans. Ultrason. Ferroelectr. Freq. Control **43**, 956–969 (1996).
[12] R. Lavarello and M. Oelze, "Density imaging using inverse scattering," J. Acoust. Soc. Am. **125**, 793–802 (2009).